Available online at www.sciencedirect.com

ScienceDirect

Energy Procedia 94 (2016) 82 – 101

Energy Procedia

13th Deep Sea Offshore Wind R&D Conference, EERA DeepWind'2016, 20-22 January 2016, Trondheim, Norway

OC5 Project Phase Ib: Validation of Hydrodynamic Loading on a Fixed, Flexible Cylinder for Offshore Wind Applications

Amy N. Robertson[a]*, Fabian Wendt[a], Jason M. Jonkman[a], Wojciech Popko[b], Michael Borg[c], Henrik Bredmose[c], Flemming Schlutter[d], Jacob Qvist[e], Roger Bergua[f], Rob Harries[g], Anders Yde[c], Tor Anders Nygaard[h], Jacobus Bernardus de Vaal[h], Luca Oggiano[h], Pauline Bozonnet[i], Ludovic Bouy[j], Carlos Barrera Sanchez[k], Raul Guanche García[k], Erin E. Bachynski[l], Ying Tu[m], Ilmas Bayati[n], Friedemann Borisade[o], Hyunkyoung Shin[p], Tjeerd van der Zee[q], Matthieu Guerinel[r]

[a]*National Renewable Energy Laboratory, USA*
[b]*Fraunhofer IWES, Germany*
[c]*Technical University of Denmark, Denmark*
[d]*Danish Hydraulic Institute, Denmark*
[e]*4Subsea, Norway*
[f]*GE Renewable Energy, Spain*
[g]*DNV GL, England*
[h]*Institute for Energy Technology, Norway*
[i]*IFP Energies nouvelles, France*
[j]*PRINCIPIA, France*
[k]*Universidad de Cantabria – IH Cantabria, Spain*
[l]*MARINTEK, Norway*
[m]*Norwegian University of Science and Technology, Norway*
[n]*Politecnico di Milano, Italy*
[o]*Stuttgart Wind Energy, University of Stuttgart, Germany*
[p]*University of Ulsan, Korea*
[q]*Knowledge Centre WMC, the Netherlands*
[r]*WavEC Offshore Renewables, Portugal*

* Corresponding author. Tel.: +1-303-384-7157.
E-mail address: amy.robertson@nrel.gov

Peer-review under responsibility of SINTEF Energi AS
doi:10.1016/j.egypro.2016.09.201

Abstract

This paper summarizes the findings from Phase Ib of the Offshore Code Comparison, Collaboration, Continued with Correlation (OC5) project. OC5 is a project run under the International Energy Agency (IEA) Wind Research Task 30, and is focused on validating the tools used for modelling offshore wind systems through the comparison of simulated responses of select offshore wind systems (and components) to physical test data. For Phase Ib of the project, simulated hydrodynamic loads on a flexible cylinder fixed to a sloped bed were validated against test measurements made in the shallow water basin at the Danish Hydraulic Institute (DHI) with support from the Technical University of Denmark (DTU). The first phase of OC5 examined two simple cylinder structures (Phase Ia and Ib) to focus on validation of hydrodynamic models used in the various tools before moving on to more complex offshore wind systems and the associated coupled physics. Verification and validation activities such as these lead to improvement of offshore wind modelling tools, which will enable the development of more innovative and cost-effective offshore wind designs.

Peer-review under responsibility of SINTEF Energi AS

Keywords: Verification, validation, monopile, cylinder, hydrodynamics, offshore wind

1. Introduction

Offshore wind turbines (OWTs) are designed and analyzed using comprehensive simulation tools (or codes) that account for the coupled dynamics of the wind inflow, aerodynamics, elasticity, and controls of the turbine, along with the incident waves, sea current, hydrodynamics, mooring dynamics, and foundation dynamics of the support structure. The OC3 and OC4 projects (Offshore Code Comparison Collaboration and Offshore Code Comparison Collaboration Continuation), which operated under IEA Wind Tasks 23 and 30, were established to verify the accuracy of OWT modelling tools through code-to-code comparisons. These projects were successful in showing the influence of different modelling approaches on the simulated response of offshore wind systems. Code-to-code comparisons, though, can only identify differences. They do not determine which solution is the most accurate. To address this limitation, an extension of Task 30 was initiated, which is called OC5. This project's objective is validating offshore wind modelling tools through the comparison of simulated responses to physical response data from actual measurements. The project will involve three phases using data from both floating and fixed-bottom systems, and from both scaled tank testing and full-scale, open-ocean testing.

The first phase of OC5 is focused on examining the hydrodynamic loads on fixed cylinders. No wind turbine is present in these tests because the purpose is to examine hydrodynamic loads only, before moving on to the complexity of coupled wind/wave loads and dynamic system response. Because this is the first time the group has used measured test data, a simple structure is chosen to ease into the complications involved when using real data. The first phase is also used to develop the model calibration and validation processes that will be used by the group throughout the project. Two different sets of data were examined in this phase, and this paper focuses on the validation work for the second data set, which came from DHI. A summary of the work done on the first data set from MARINTEK can be found in [1]. The first data set focused on examining a fixed, rigid cylinder suspended in a wave tank, whereas the second data set uses a flexible cylinder fixed to the floor of a wave tank, and uses a sloped floor to include nonlinear wave transformation from deep water to the structure in the experiments.

A number of academic and industrial project partners from 11 different countries participated in the task. Those actively involved in Phase Ib are: the National Renewable Energy Laboratory (NREL - USA), Technical University of Denmark (DTU), MARINTEK (Norway), 4Subsea (Norway), Norwegian University of Science and Technology (NTNU - Norway), Politecnico di Milano (PoliMi - Italy), Stuttgart Wind Energy (SWE - Germany), the Institute for Energy Technology (IFE - Norway), DNV GL (UK), GE Renewable Energy (Spain), IFP Energies nouvelles (France), PRINCIPIA (France), University of Ulsan (UOU - Korea), Wave Energy Center (WavEC - Portugal), and

Knowledge Centre WMC (the Netherlands).

2. Model Test Description

The data used in this study comes from the Wave Loads project [2], a three-year project with the goal of developing improved numerical models for wave loads on offshore wind turbines. The project was carried out collaboratively by DTU Wind Energy, DTU Mechanical Engineering, and DHI. Model tests of three different cylinder specimens were performed at DHI in a sloped bed configuration. Within the OC5 project, we examined the tests performed at 1:80 scale using a flexible, fixed-bottom cylinder. Several reports are available outlining the original test program and its findings (see references [4]-[5]). The flexible-cylinder data set was analyzed in [3], which also presented numerical reproduction of the wave kinematics and structural response in terms of the fully nonlinear potential flow solver OceanWave3D [10] and a finite-element model.

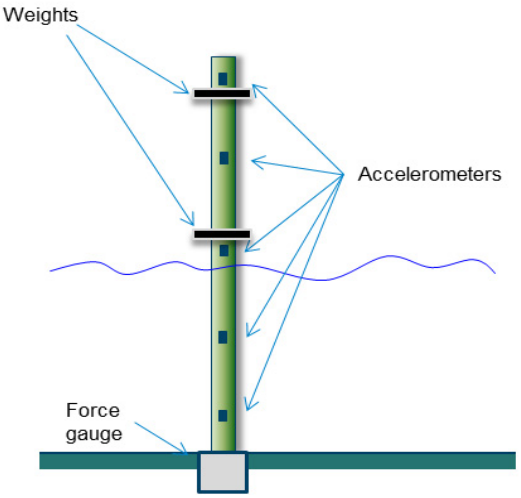

Figure 1. Drawing of test cylinder and location of sensors [2]

The properties of the 1:80-scale cylinder are given in Table 1. It has a diameter of 7.5 cm, which relates to a 6-m-diameter cylinder at full scale using a scaling factor of 80. All data presented in this paper are at model scale, unless otherwise stated. The cylinder is flexible, and is made of PVC pipe with a wall thickness of 1.8 mm. The pipe was fastened to a plug on a load cell at the seabed and two weights were mounted on the pipe (see Figure 1) to match the two first natural frequencies of the OC3 monopile [6]. Having a flexible cylinder allowed for the study of wave-driven excitation including springing, ringing, and impulsive excitation. Two different water depths were considered.

Table 1. Properties of the flexible cylinder (Model scale based on Froude scaling)

	Model Scale (1:80)	**Full Scale**
Water depth of cylinder	0.51 m and 0.26 m	40 m and 20 m
Water depth of wave maker	0.78 m and 0.53 m	15.6 m
Cylinder diameter	7.5 cm	6.0 m
Cylinder height	200 cm	160 m
Wall thickness	1.8 mm	0.144 m
Young's modulus (E)	3.7 GPa	296 GPa
EI (I = moment of inertia)	1026 N-m^2	4.2e10 N-m^2
Density	0.64 kg/m	4.2e3 kg/m
Mass m1	1.786 kg	937e3 kg
Mass m2	1.784 kg	936e3 kg
Mass m1 height, h1	160.75 cm	128.6 m
Mass m2 height, h2	108.75 cm	87.0 m
Natural frequency, f1	2.5 Hz	0.28 Hz
Natural frequency, f2	18 Hz	2.0 Hz
Damping ratio, f1	0.017	0.017
Damping ratio, f2	0.027	0.027

The tests were performed in the shallow water basin at DHI. The basin has a size of 35 m x 25 m and is equipped with a three-dimensional (3-D) wave maker at one end. One of the goals of the project was to study breaking waves. To achieve steep and breaking waves by natural shoaling at the water depths tested, a slope of 1:25 was built in front of the wave maker, extending to a plateau. A rock berm was built at the down-wave end of the basin to absorb

waves and reduce reflection (see Figure 2). Models were placed both on the slope and on the horizontal portion (see Figure 2). The OC5 group studied tests in which the cylinder was placed on the slope, at a distance of 7.75 m from the wave maker.

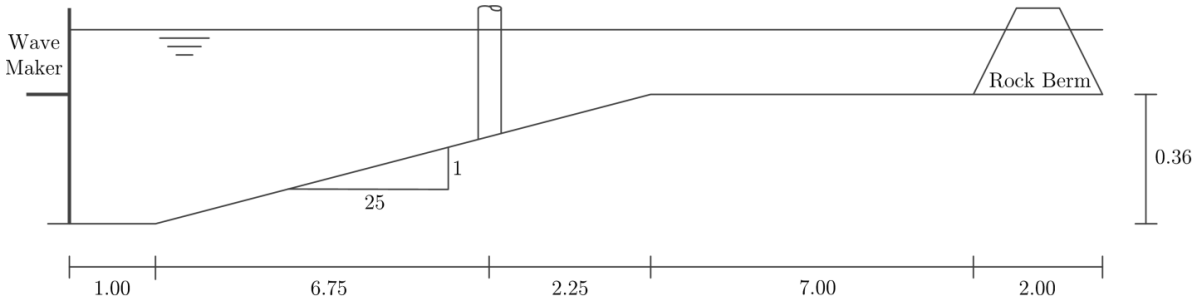

Figure 2. Side view of water tank and test cylinder locations [2]

Seven different test series were provided to the OC5 project for analysis, and are summarized in Table 2. The table provides a description of the water depth, wave height (H) or significant wave height (Hs), wave period (T) or peak-spectral wave period (Tp), the added mass coefficient (C_A), and drag coefficient (C_D) for each of the test cases (see Section 3 for an explanation of the choice for the added mass and drag coefficients). The data are from tests performed at two different water depths, 0.51 m and 0.26 m, with the shallow water of the latter resulting in highly nonlinear wave profiles. For each of the two water depths, a variety of regular and irregular wave tests were examined. For each of the tests, measurements were provided for the wave elevation (at 21 locations), flow velocity, connection force between the cylinder and the seabed (hereafter denoted as the bed shear force), acceleration at five locations, and the horizontal displacement of the cylinder at the level of the upper mass. For the validation work, only the wave measurement beside the cylinder was used, as well as the bed shear force and acceleration at a level of 165 cm above the seabed.

Table 2. Data sets simulated in OC5 project, Phase Ib

Test #	Wave Type	Water Depth (m)	H/Hs (m)	T/Tp (s)	Gamma	C_A	C_D
1	Regular	0.51	0.090	1.5655		1.22	1.0
2	Regular	0.51	0.118	1.5655		1.22	1.0
3	Irregular	0.51	0.104	1.40	3.3	1.0	1.0
4	Irregular	0.51	0.140	1.55	3.3	1.0	1.0
5	Regular	0.26	0.086	1.565		1.22	1.0
6	Regular	0.26	0.121	1.565		1.22	1.0
7	Irregular	0.26	0.133	1.560	3.3	1.0	1.0

3. Calibration and Validation Procedure

The goal of the OC5 Phase Ib analysis was to validate the ability of offshore wind modelling tools to predict the measured hydrodynamic loads and acceleration of a flexible cylinder in a variety of wave conditions. The first step towards achieving this goal was to calibrate a model of the system, which is necessary when there are uncertainties in the model parameters or measured quantities.

For this set of experiments, the geometry of the system was well known, but there were some uncertainties related to the wave elevation, load, and acceleration measurements. During initial investigations, the untuned

simulation models predicted hydrodynamic loads that were lower than the measurements. The reasons for this difference between the measured and modelled hydrodynamic loads could be deficiencies in the simulation models, poor calibration/resolution of the force measurement device, or unmodelled hydrodynamic conditions such as the presence of reflected waves off the walls of the tank. The group's suspicion was that reflected waves (or some other unmeasured/unmodelled wave condition) was the most likely cause of the difference, because the modelling approaches employed have been shown to work well for the deep water conditions of Tests 1-4, and because the force measurement device was well-tuned and calibrated. Participants therefore used Test 1 to calibrate the hydrodynamic coefficients for the simulation models by examining what values for the coefficients produced force levels similar to the test. The group wanted to use consistent values between simulation tools, and therefore an average value for the coefficients was chosen based on the tuning results from all participants. A value of 1.22 was chosen for the added mass coefficient (C_A), and 1.0 was chosen for the drag coefficient (C_D) to obtain the loading levels seen in the tests. Although the drag coefficient is consistent with modelling theory, the added mass coefficient is higher than theory would suggest, again likely due to the presence of unmodelled, reflected waves. These calibrated values were then used for the remainder of the regular wave test cases by all participants. Tuning was more difficult for the irregular wave tests, and so a standard value of 1.0 was used for both C_A and C_D. Having all participants use the same coefficients allowed for easier comparison of the influence of different modelling approaches.

No calibration was done for the acceleration measurement. A prescribed structural damping value was provided to participants for the first two bending frequencies of the structure, based on analysis of hammer tests. However, there was an issue in this measurement related to the compliance of the load sensor from its mounting on the tank floor. This compliance introduced a natural frequency in the system around 50 Hz. Although this frequency is far from the wave-frequency range, steep waves were able to excite it and create a large amount of motion in the cylinder. To alleviate its influence, the acceleration measurements were low-pass filtered using a Butterworth filter at 30 Hz.

4. Modelling Approach

A list of the tools used in this study is provided in Table 3, which also shows the participant using the tool, and the modelling approach employed. Many of these tools are fairly new, but are based on well-established methods for modelling hydrodynamic loads. Other tools are ones that have been used extensively in the offshore industry, but have been modified or coupled to other software packages to enable the modelling of the aerodynamic turbine loads. The purpose here is to understand the different capabilities of these tools and how modelling choices affect the accuracy of their calculated hydrodynamic loads before moving on to systems with more complex geometry and coupling with turbine aerodynamic loads and control.

The experiment examined here is fairly simple in that there is no wind turbine present and the structure has a simple cylindrical geometry with no shadowing effects. This allows us to focus on the influence of the wave theory and hydrodynamic load model on the calculated reaction loads. Because of the simplicity of the problem, most of the participants chose to use a modelling approach consisting purely of Morison's equation (see [7]). For a fixed, rigid cylinder, Morison's equation is written as:

$$F = \frac{1}{2} C_D \rho D u |u| + C_M \rho \frac{\pi D^2}{4} \dot{u} \tag{1}$$

where u is the x-velocity of the fluid normal to the cylinder, $\dot{u}$ is the fluid acceleration normal to the cylinder, D is the cylinder diameter, ρ is the fluid density, C_D is the drag coefficient, C_M is the inertia coefficient ($C_A = C_M$-1), and F is the force per unit length on the cylinder. (Most participants used the relative form of Morison's equation, accounting for the relative motion between the fluid and vibrating structure.) Morison's equation has been used extensively throughout the offshore community for calculating hydrodynamic loads (see, for example, [8] and [9]), and the purpose of this study is to understand how the different capabilities available in offshore wind modelling tools will affect the resulting force calculation and how to best choose the parameters in the equation.

In addition to Morison's equation, some participants used potential flow (PF) theory via a panel method approach to model the hydrodynamic loads (augmented with the viscous-drag term from Morison's equation). In the tools utilized, the PF approach could not account for the deflection of the structure when computing the hydrodynamic loads; in these cases, the cylinder was considered as rigid.

Table 3. Summary of offshore wind modelling tools and modelling approach

Participant	Code	Wave Model (Reg/Irr)	Wave Elevation	Hydro Model	Structural Model	Number DOFs
4Subsea	OrcaFlex	FNPF kinematics	FNPF kinematics	ME	FE, RDS	160 elements 960 DOFs
GE	Samcef Wind Turbines	5th-Order Stokes/ Linear Airy	Stretching	ME	FE (TS), RD	13 elements 84 DOFs
DNV GL-ME	Bladed 4.6	6th- and 8th-Order SF/ Linear Airy	Measured	ME	FE (TS), MD	8 (CB)
DNV GL-PF	Bladed 4.6	Linear Airy	Measured	1st Order PF	Rigid	N/A
DTU-HAWC2	HAWC2	6th-and 8th-Order SF/Linear Airy and FNPF kinematics	Stretching and FNPF kinematics	ME	FE (TS), RDS	20 elements, 126 DOFs
DTU-HAWC2-PF	HAWC2	6th-and 8th-Order SF/Linear Airy	Stretching	McCamy & Fuchs	FE (TS), RDS	31 elements, 192 DOF
DTU-BEAM	OceanWave3D	FNPF kinematics	FNPF kinematics	ME+Rainey	FE (EB), RD	160 DOFs
IFE	3Dfloat	FNPF kinematics	FNPF kinematics	ME	FE (EB), RDS	62 elements, 378 DOFs
IFE-CFD	STAR CCM	CFD	CFD-derived	CFD	Rigid	N/A
IFP-PRI	DeeplinesWind	3rd-Order SF/ Linear Airy	Measured	ME	FE	200 elements
UC-IHC	IH2VOF	FNPF kinematics	FNPF kinematics	ME	Rigid	N/A
MARINTEK	RIFLEX	2nd-Order Stokes and FNPF kinematics	Measured and FNPF kin.	ME	FE(E-B), RDS, FS	167 elements, 1002 DOFs
NREL-ME	FAST	2nd-Order Stokes and FNPF kinematics	Measured and FNPF kin.	ME	FE (TS), MD	4 (CB)
NREL-PF	FAST	2nd-Order Stokes	Measured	2nd-Order PF	Rigid	N/A
NTNU-Lin	FEDEM 7.1	Linear Airy	None	ME	FE (EB), RD	13 elements, 84 DOFs
NTNU-Stokes5	FEDEM 7.1	5th-Order Stokes	None	ME	FE (EB), RD	13 elements, 84 DOFs
NTNU-Stream	FEDEM 7.1	Stream Function	None	ME	FE (EB), RD	13 elements, 84 DOFs
PoliMi	POLI-HydroWind	2nd-Order Stokes	None	ME	FE (EB), RD	23 elements, 69 DOFs
SWE	SIMPACK +HydroDyn	2nd-Order Stokes	None	ME	FE (TS), MD	50
UOU	UOU + FAST	2nd-Order Stokes	None	ME	Rigid	N/A
WavEC	Wavec2Wire	2nd-Order Stokes	Measured	2nd-/1st-Order PF	Rigid	N/A
WMC	FOCUS6 (PHATAS)	FNPF kinematics	FNPF kinematics	ME	FE (TS), MD	12 (CB)

In addition to the hydrodynamic model employed, differences between the participants' modelling approaches are related to the utilized wave model. The different wave theories employed are shown in the 'Wave Model' column in Table 3, whereas the 'Wave Elevation' column indicates additional information regarding how the wave theory was employed. For the wave model itself, participants used a variety of approaches including linear Airy waves and higher-order models such as 2nd- and 5th-order Stokes theory, 3rd-order Dean waves, and 3rd-, 6th-, and 8th-order stream functions (SFs). Linear Airy wave theory only calculates the wave kinematics up to the mean sea level of the water, and so some participants used stretching procedures so that wave loads would be calculated up to the instantaneous water level (indicated by "stretching" in the 'Wave Elevation' column). Some participants computed the wave elevation while others chose to directly input the measured wave elevation time history in their simulation to capture the time-varying nature of the wave and its higher-order characteristics (indicated by "measured" in the 'Wave Elevation' column). For participants using the measured wave elevation, the indicated wave theory was used to calculate the distributed wave velocities and accelerations (wave kinematics) across the length of the cylinder, as these were not measured. For NREL, two wave elevation solutions are provided. "Elv1" uses the wave elevation directly and computes the wave kinematics using 1st-order Airy wave theory, whereas "elv2" first band-pass filters the measured wave elevation to the main linear frequency range and then adds the 2nd-order kinematics computed for that range. This approach can be seen as an ad-hoc alternative to the method of [11]. One participant (IFE) also used a computational fluid dynamics (CFD) tool.

Additionally, some chose to use wave kinematics derived from a fully nonlinear potential-flow (FNPF) solver (indicated by "FNPF kinematics" in the 'Wave Elevation' column) to better approximate the influence of the sloped seabed on the generated waves. The FNPF-derived kinematics were calculated by DTU using their OceanWave3D tool [10], and were input into participants' modelling tools, bypassing the generation of the kinematics using a prescribed wave theory. The OceanWave3D model solves the unsteady wave problem by time stepping the fully nonlinear free-surface boundary conditions for the free-surface elevation. In each time step, the 3-D Laplace equation is solved by a multigrid approach to provide the vertical particle velocity. The regular wave test kinematics were computed in a numerical domain resembling that of the physical test (Figure 2), imposing the wave paddle velocity of the tests at the left boundary. For the irregular test cases, where not all paddle signals were available, the approach of [3] was followed. Here, the linear wave field was constructed in the deep part of the domain by linear analysis of four wave gauge signals. Next, the linear wave field was imposed in a relaxation zone placed at the left side of the paddle position.

Because the cylinder for these experiments was flexible, the structural dynamics model employed could also have an influence on the measured force and acceleration of the cylinder. In the 'Structural Model' column, the different structural modelling approaches employed are described, which include either a finite-element (FE) approach or just a rigid model. Most models using potential-flow theory must use a rigid structural model as the hydrodynamic force calculation is performed for the undeflected position. The FE models used either Euler-Bernoulli (EB) or Timoshenko (TS) beam elements, with either modal damping (MD) or Rayleigh damping (RD)—with some employing just stiffness-proportional Rayleigh damping (RDS). The number of elements and degrees of freedom (DOFs) used in the structural models is also given, with some using Craig-Bampton (CB) reduction techniques. One group, MARINTEK, chose to model the system at full scale (FS) rather than model scale.

5. Results

The accuracy of the modelling tools introduced in the last section for predicting the hydrodynamic loads and acceleration response of a flexible cylinder for a variety of wave conditions was validated through the simulation of the seven data sets summarized in Table 2, and the comparison of the simulated response to measured test data from DHI. For each of these tests, with the exception of Test 1 (calibration test case), only the wave time history was provided to the participants. Participants were asked to report the total measured bed shear force on the cylinder and associated acceleration response 165 cm above the seabed for each of the tests when using the prescribed hydrodynamic coefficients, wave elevations, and wave periods given in Table 2. Some participants deviated from the specified wave parameters by directly entering the measured wave time history or by using FNPF-derived wave kinematics.

Some examples of the comparisons between the measured and simulated force time histories are given in Figure

3 and Figure 5 for Test 1 and Test 6, respectively. The top image in these figures shows an excerpt of the time history of the bed shear force, and the bottom figure shows the power spectral density (PSD) of the total force record. For Test 1, the force time history is fairly linear, and the tools are (in general) predicting the force time history well (as expected due to the calibration of C_A). More differences are seen for Test 6, which is performed at a shallower water depth and with a larger wave height, thus creating more nonlinear waves and more nonlinear forces on the cylinder. The degree of nonlinearity can be seen by the size of the peaks in the PSD at the harmonics of the wave frequency, which are quite large for Test 6, but barely visible for Test 1. The acceleration response at the top mass level of the cylinder for Test 1 is given in Figure 4 and shows a large peak at 2.5 Hz, which is the first bending mode of the cylinder.

Color and line definition schemes are used in these plots to differentiate between different modelling approaches. Those using a linear wave modelling theory are indicated by varying shades of red, those using a 2nd-order modelling theory are indicated in blues, and higher-order wave modelling theories are in green. Tools with these colors use a Morison equation (ME) hydrodynamic model. Those using a potential-flow model are indicated by varying shades of orange, those using CFD or a stream function are indicated by varying shades of gray, and those using DTU-prescribed FNPF kinematics are indicated by varying shades of brown. The line definition further identifies those using internally computed wave kinematics (dashed) versus those using the measured wave elevation (dash-dot) or CFD/FNPF-derived kinematics (solid). The label "kin" (for CFD or FNPF-derived kinematics) or "elv" (for using the measured wave elevation) is also added to the end of the names of the participants to indicate this delineation.

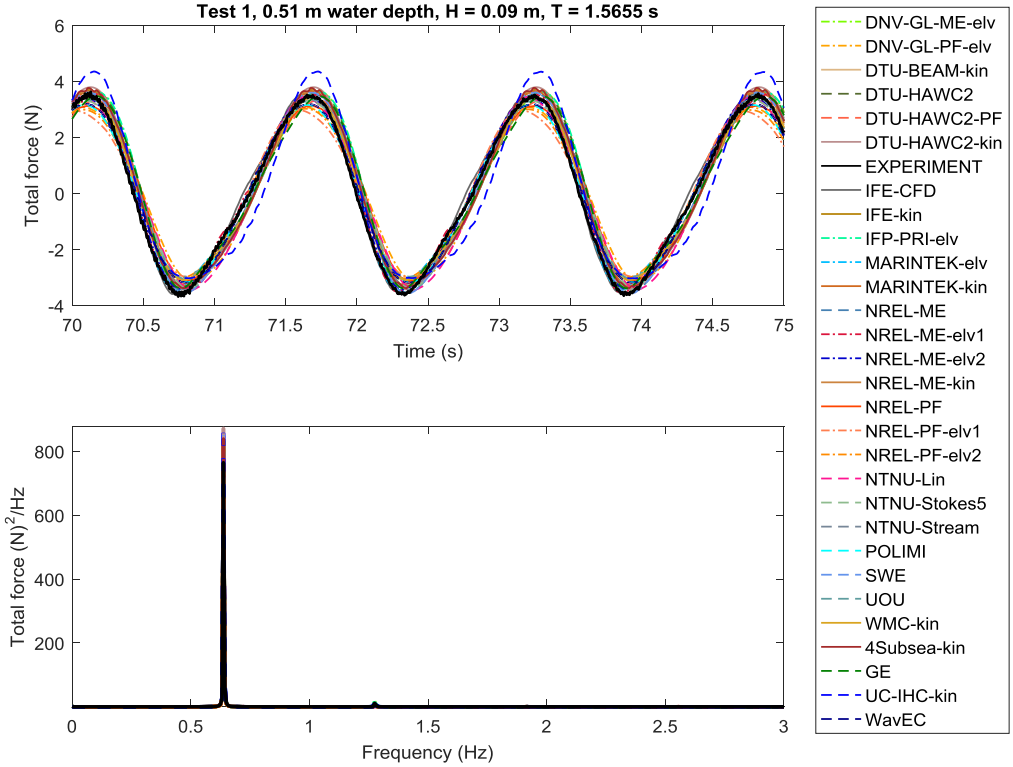

Figure 3. Validation of force time histories and associated PSDs for Test 1 against the experimental measurement

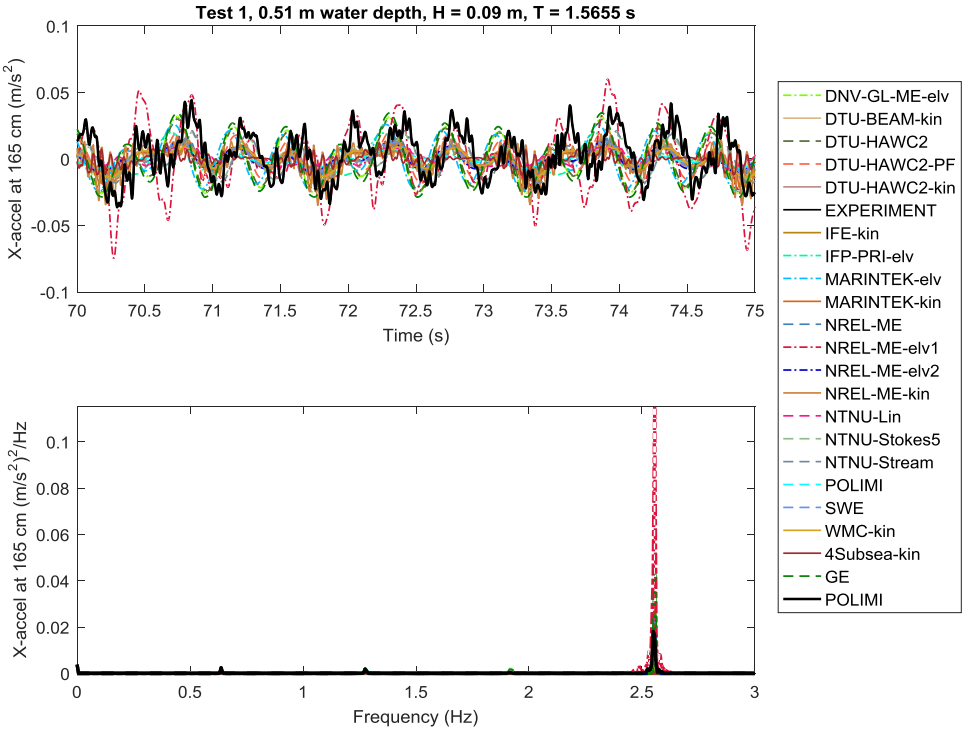

Figure 4. Validation of acceleration response and associated PSDs for Test 1 against experimental measurement

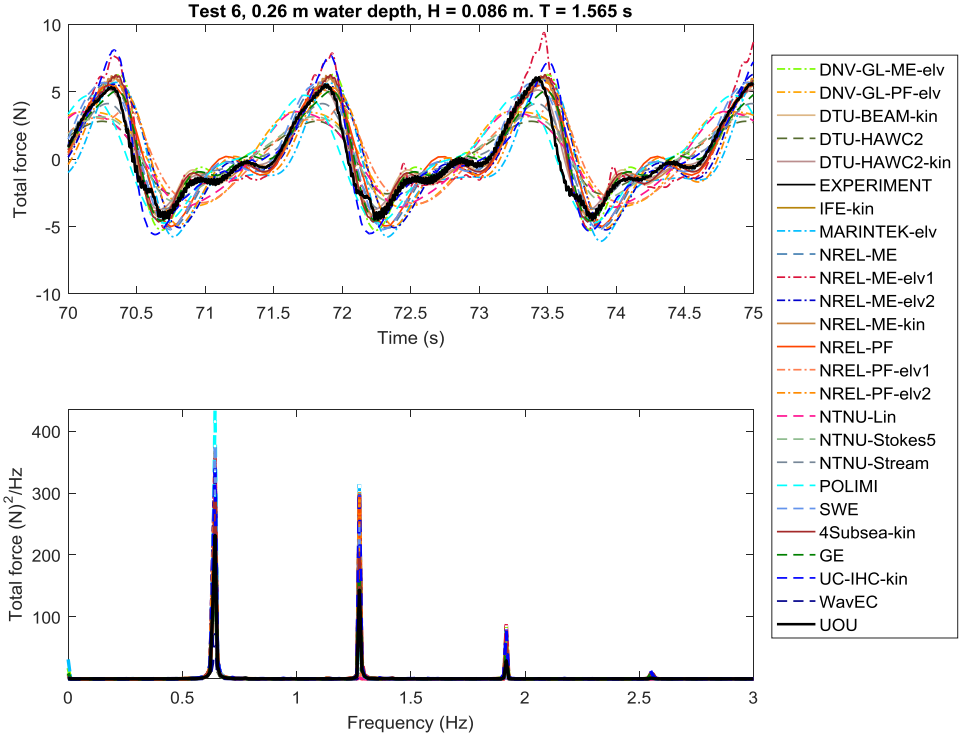

Figure 5. Validation of force time histories and associated PSDs for Test 6 against the experimental measurement

5.1. Regular Waves

To better examine the differences in the calculated forces between the modelling tools for the regular wave cases (Tests 1, 2, 5, and 6), bar plots of the maximum measured force are compared in Figure 6. These plots show that the maximum (overall) force for the tests performed in deeper water (Tests 1 and 2) is fairly consistent between the modelling tools, and is similar to the experimental measurement. There is less agreement for the shallower water depth (Tests 5 and 6). One of the reasons for differences between the simulated and measured forces is that linear wave models tend to underpredict the peak force because real waves have higher peaks and shallower troughs than a linear sinusoidal signal. The observed differences between tools using ME and those using PF are potentially related to the fact that the added mass coefficient (C_A) in the ME model was tuned to better estimate the forces measured in the test, which were probably larger than expected because of reflected waves that were not included in the simulations. Those using PF theory, however, could not as easily tune their added mass and therefore are underpredicting the measured force. In addition, those using a PF approach assume the structure as rigid. The acceleration of a flexible body will cause an added contribution to the measured shear force at the root due to inertia loads. Depending on the frequency content of the forcing signal and the stiffness of the structure, this can lead to either an under- or overprediction of the root shear force.

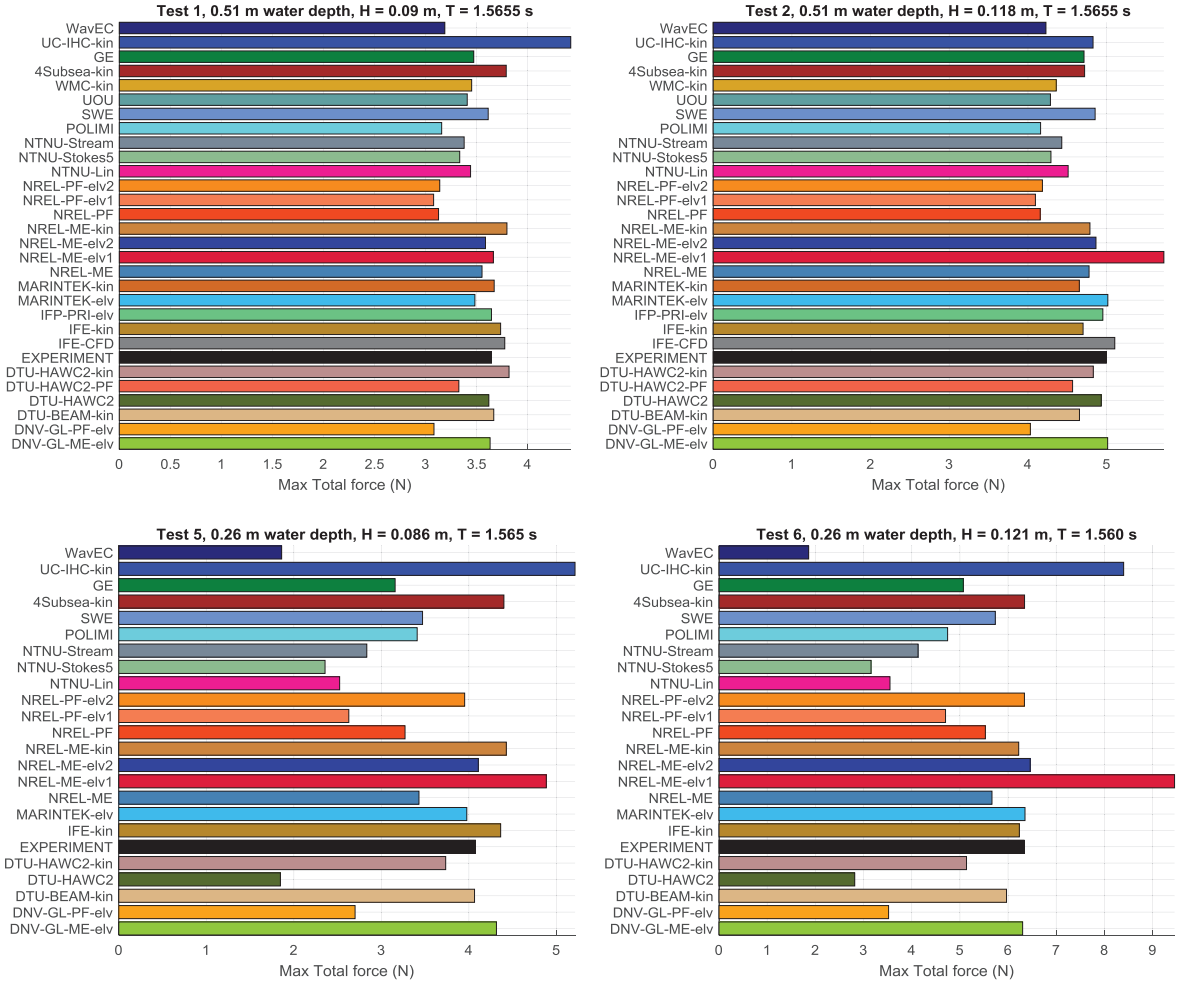

Figure 6. Validation of simulated maximum total forces for regular wave tests against the experimental measurement

The overall force magnitude (maximum) is predicted better for Test 1 and 2 because these signals are fairly linear, and most modelling approaches are able to capture the linear portion of the wave elevation and resulting force fairly well. More differences arise from how tools model/treat the higher-order components of the wave elevation model and force computation, which is evident by the larger differences seen for the maximum force for Tests 5 and 6, wherein shallower water depths create more nonlinear wave signals. To look more closely at the higher-order components of the force simulations and measurement, the 1st, 2nd, and 3rd peaks of the force PSD signal (as shown in Figure 5 for Test 6) are compared between the experiment and participants. This component is calculated by integrating the force PSD over a band covering the given frequency peak and then taking the square root, which should equate to the equivalent magnitude of the 1st, 2nd, and 3rd wave harmonic contributions to the force signal. This comparison is shown in Figure 7 through Figure 9.

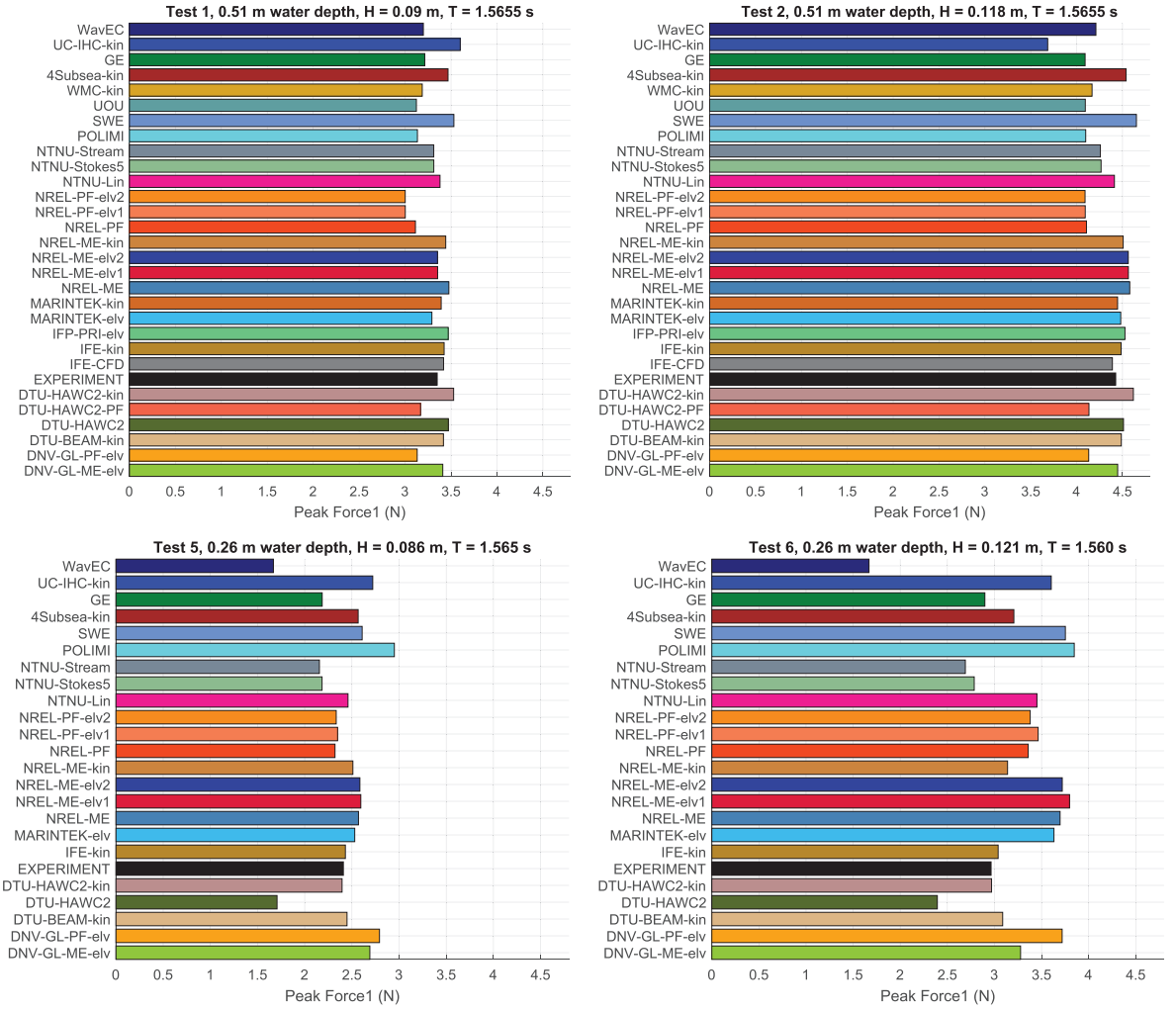

Figure 7. Validation of simulated magnitude of 1st peak of force PSD against the test measurement

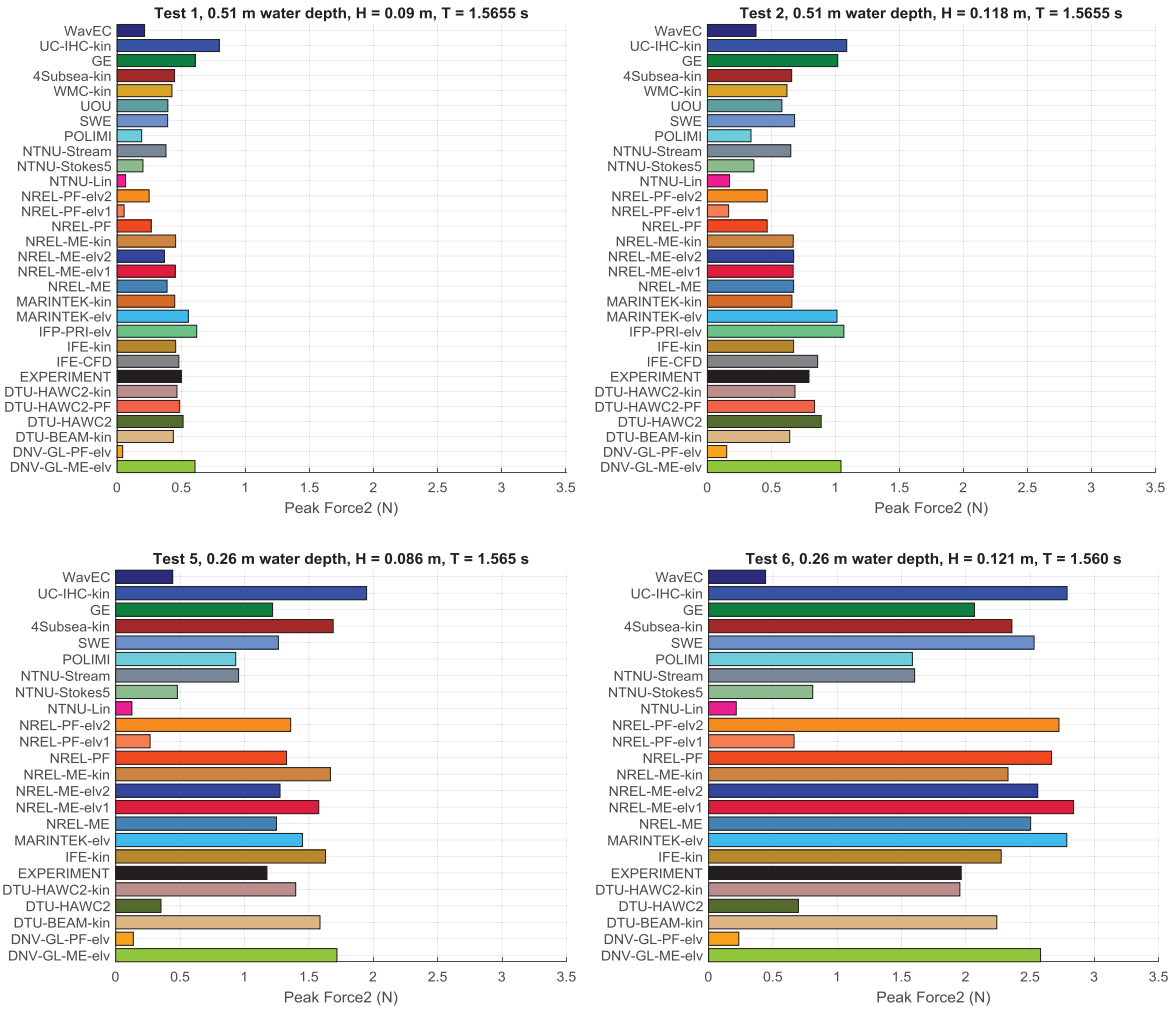

Figure 8. Validation of simulated magnitude of 2nd peak of force PSD against the test measurement

Because the majority of the force magnitude comes from the 1st peak of the force signal (especially for Tests 1 and 2), the comparison of the 1st-force peak components in Figure 7 is similar to those of the overall force magnitude (or maximum) shown in Figure 6. There is less variation between modelling tools for the 1st peak of the force for Tests 5 and 6 than the maxima because the higher-order components do not affect its calculation. This figure, and the other force peak figures, is scaled so that all test cases are on the same scale to see the relative significance of the harmonics for the different wave conditions. More significant differences between simulation results are seen in Figure 8, which shows the magnitude of the 2nd-force peak component of the force signal. The first thing to notice here is that the magnitude of this component is very small for the deeper water conditions of Test 1 and 2. Second, those using a linear wave model (NTNU-Lin, NREL-PF-elv1, DNV-GL-PF, ABS) are capturing very little of this peak (if any). Overall, participants using either the measured wave elevation (elv) or FNPF-derived wave kinematics (kin) are closest to the measured values from the experiment. Similar conclusions can be drawn for the 3rd-force peak component in Figure 9, which includes contributions both from wave excitation and viscous drag. Although the values of the nonlinear contributions for some of the wave profiles may not be large, they have the possibility of exciting natural frequencies in the structure, thereby producing fatigue issues such

as ringing and springing.

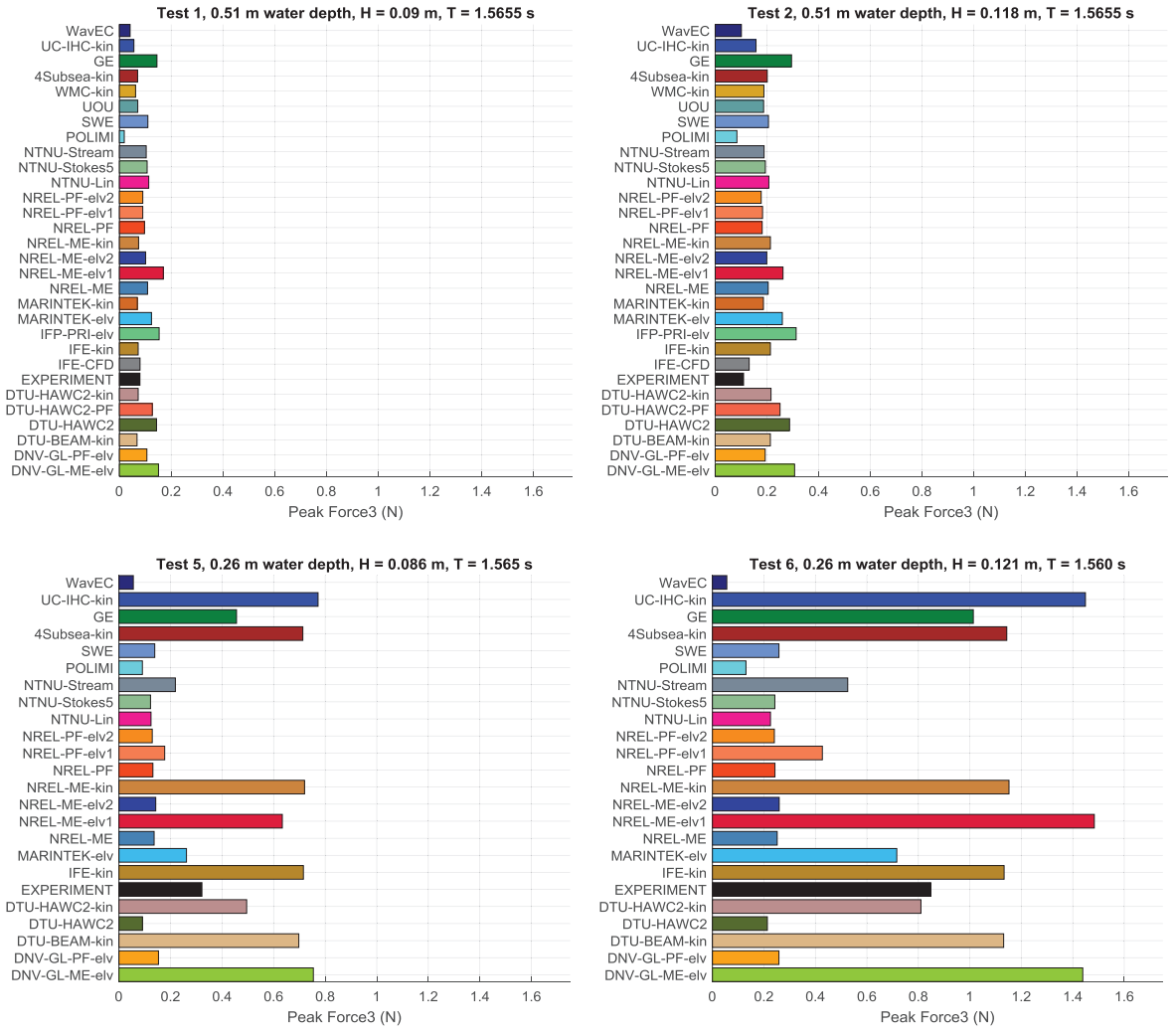

Figure 9. Validation of simulated magnitude of 3rd-peak of force PSD against the test measurement

The maximum values of the acceleration response at 165 cm above the seabed for the simulations and experiment are shown in Figure 10. There is much more variation in these results between the tools and the experiment than what was observed for the force signal, with most tools underpredicting the peak magnitude. The level of variation in these results makes it difficult to determine a set reason for the differences. It can be noted, though, that although the bed shear force is the sum of the external hydrodynamic force and the inertia force associated with dynamics of the moving structure, the accelerations are a direct measurement of the structural motion. This motion is affected by the vertical variation of the exciting force, its frequency content, and the damping of the structure. These added parameters provide more complexity and can explain the much larger level of variation. More information can be discerned from the distribution of the acceleration response, which will be examined in the next section for the three irregular wave cases.

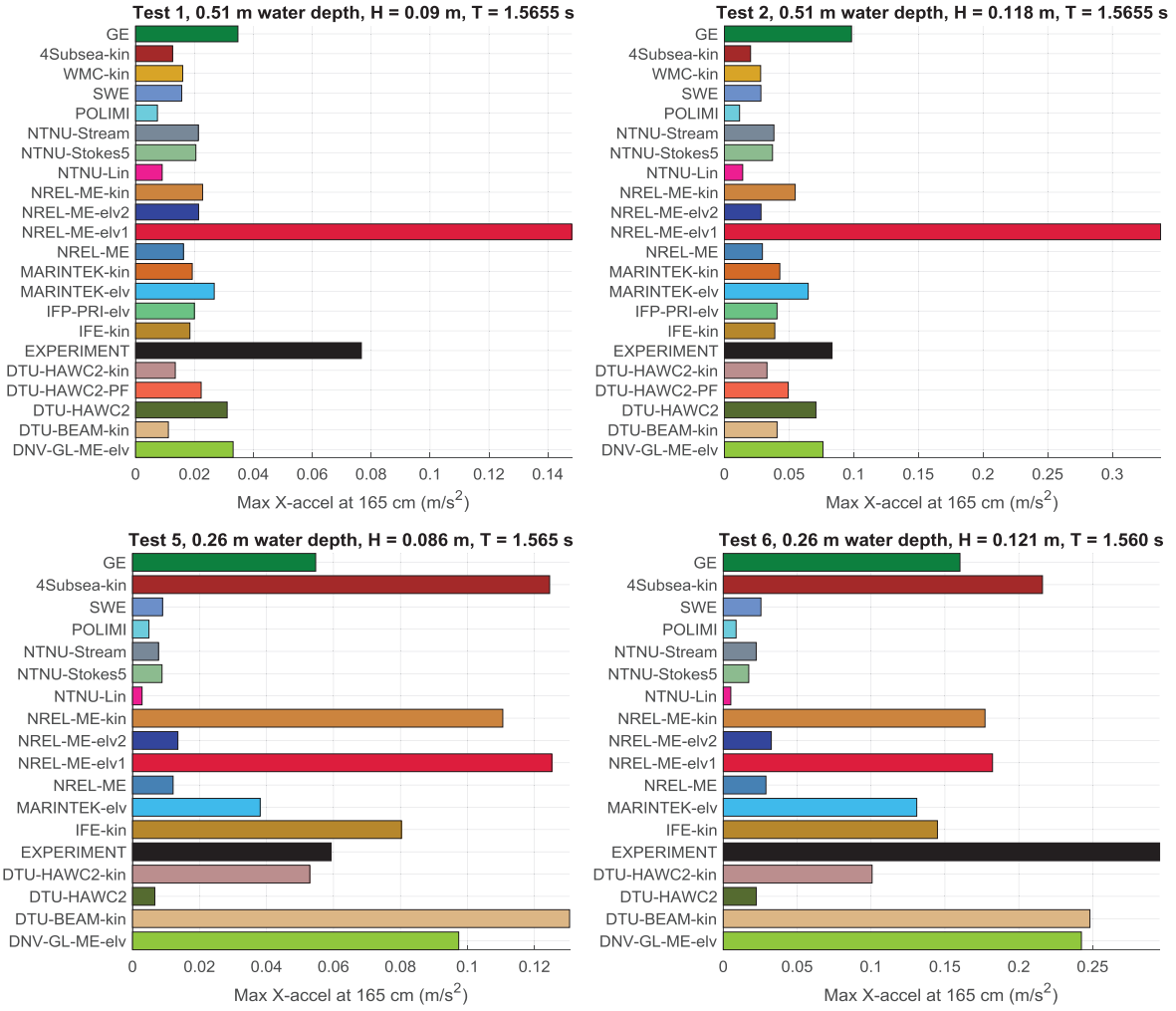

Figure 10. Validation of the simulated maximum total acceleration responses for the regular wave tests against the experimental measurement

5.2. Irregular Waves

For the irregular wave test cases (Tests 3, 4, and 7), two of the tests were performed at the larger water depth of 0.51 m, and one was performed at the shallow water depth of 0.26 m. Sections of the time histories of the wave elevation and resulting force and acceleration response for Test 3 and Test 7 can be seen in Figure 11 and Figure 12, respectively. Included in these plots are only those participants that are using either the measured wave time history or CFD/FNPF-derived kinematics, and their comparison to the experimental measurement. The modelling tools are able to capture the very nonlinear behavior of the wave elevation and resulting force for these test cases, with little visible differences between the simulations and measurement. The acceleration response, on the other hand, has larger discrepancies, which could be associated with uncertainty in this measurement. For Test 3 (Figure 11), some of the simulated responses are overpredicting the acceleration response at times, especially for steep wave events such as near 755 seconds. For Test 7, however, which is performed at the shallower wave depth of 0.26 m, there are multiple instances in which the experiment has a much larger force and acceleration response than the simulations. These instances can be seen in Figure 12 at around 704 and 712 seconds. Also, as stated in [3], the likely reason for the larger experimental response is that the waves are breaking at these instances, which will cause broad-band

frequency excitation in the system. Although the higher-order wave modelling approaches and FNPF-derived kinematics can capture the nonlinear nature of a breaking wave, they cannot capture the impulsive load that occurs when the wave physically breaks on the structure. Some participants are therefore looking into including an impulsive force in their modelling tools for conditions where breaking waves occur.

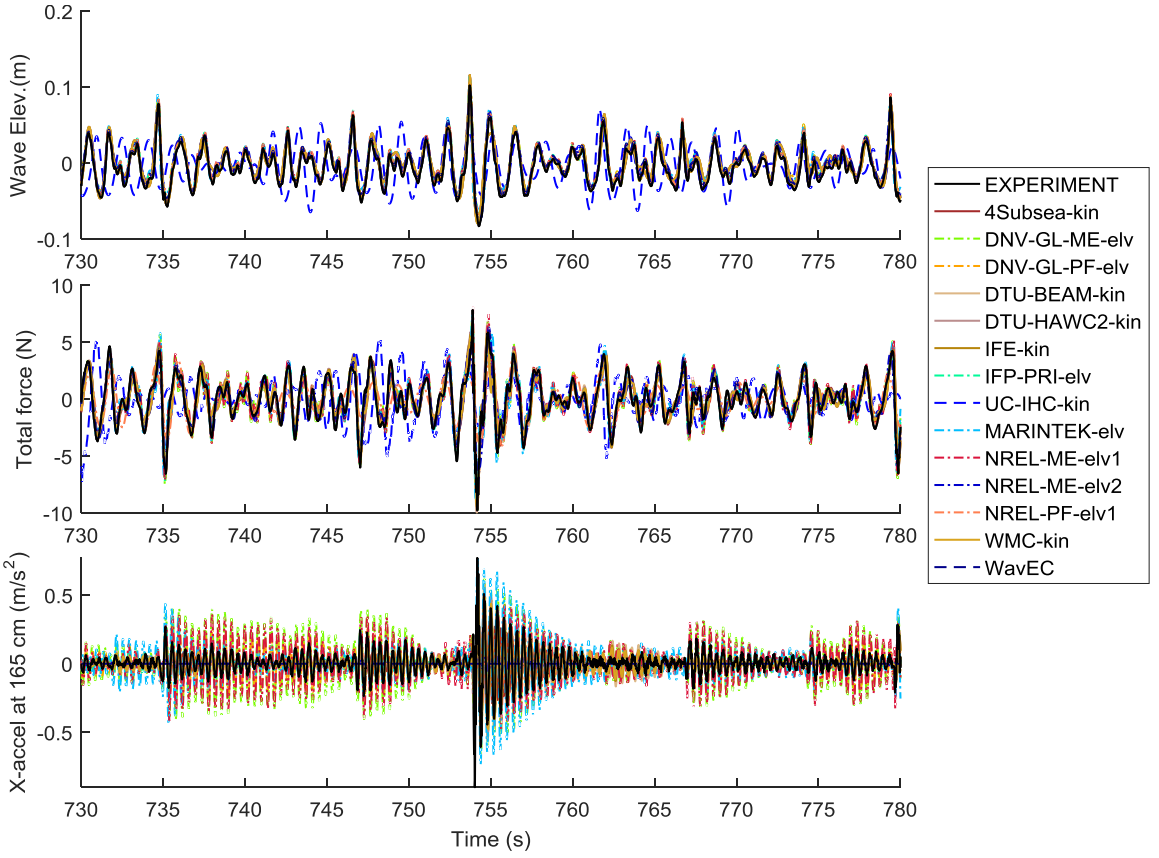

Figure 11. Validation of simulated wave elevation, force, and acceleration response against measurement for Test 3 (deeper water, irreg. waves)

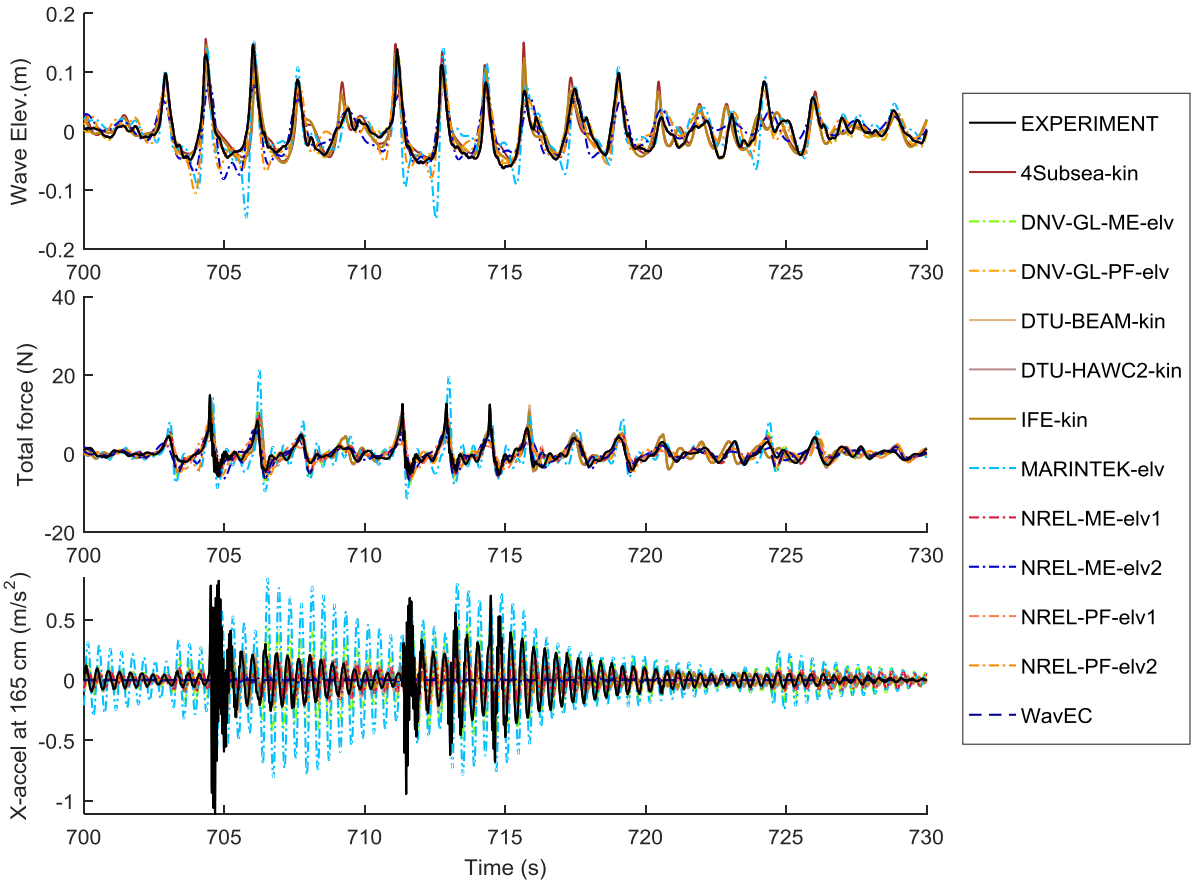

Figure 12.Validation of simulated wave elevation, force, and acceleration response against measurement for Test 7 (shallow water, irreg. waves)

To compare the levels of the individual peaks in the force and acceleration responses for the irregular load cases between the simulations and experiment, exceedance probability plots were used (see [3] for more information on this procedure). The exceedance probability plots are generated by finding the maximum in the data (force and acceleration signals) within each individual wave, defined as the time interval between two consecutive down-crossings of the surface elevation signal. Next, these points are plotted in increasing order against their probability of occurrence, essentially showing the cumulative probability distributions. The exceedance probability plots of the force and acceleration signals for the three irregular wave cases are shown in Figure 13 through Figure 15. Prior to their calculation, each of the signals was low-pass filtered using a Butterworth Filter at 30 Hz to eliminate any noise from the measurement.

For Tests 3 and 4, the force distributions were fairly consistent between the different modelling approaches, but there is less agreement for Test 7, which was performed at the shallower water depth. For this case, we start seeing that those using the CFD/FNPF-derived kinematics (results shown in brown) better approximate the force distribution of the experiment compared to those using the wave elevation measurement, or a derived JONSWAP spectrum. The reason for this is probably due to the nonlinear wave transformation over the sloped seabed, which can create unique characteristics in the wave kinematics. Standard wave theories are not able to consider the slope, but FNPF can directly model its influence, thus producing wave kinematics that are more consistent with the waves in the tank. This benefit also translates to the measured acceleration response of the system. Accurately predicting the tails of the force/acceleration curves equates to better prediction of the extremes in the data, which is essential in designing an offshore wind system.

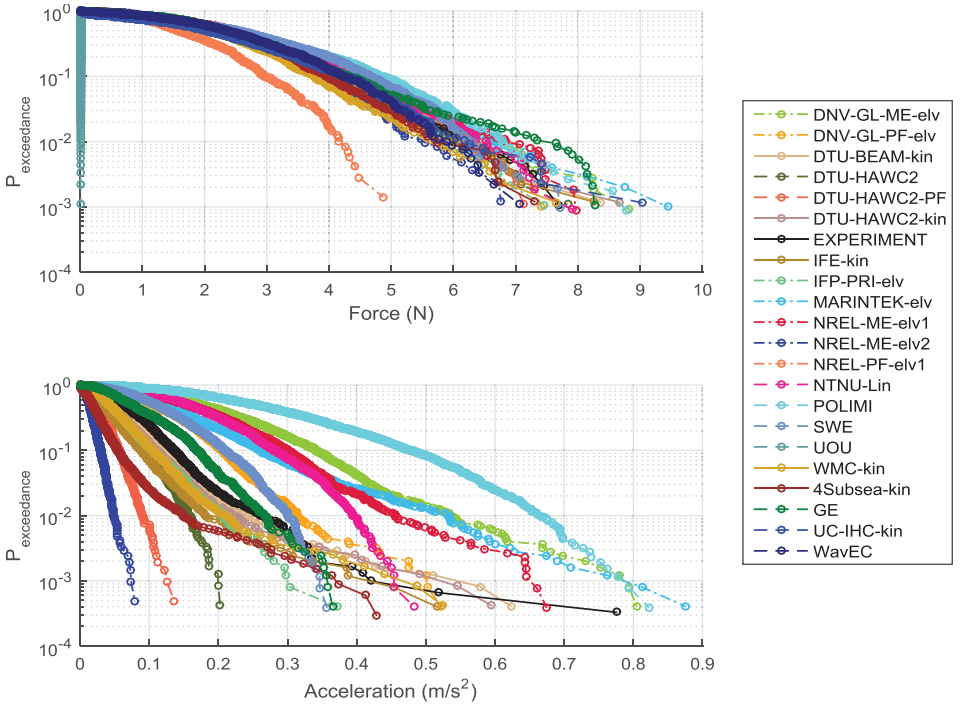

Figure 13. Validation of the simulated exceedance probabilities for the force and acceleration against test measurements (Test 3)

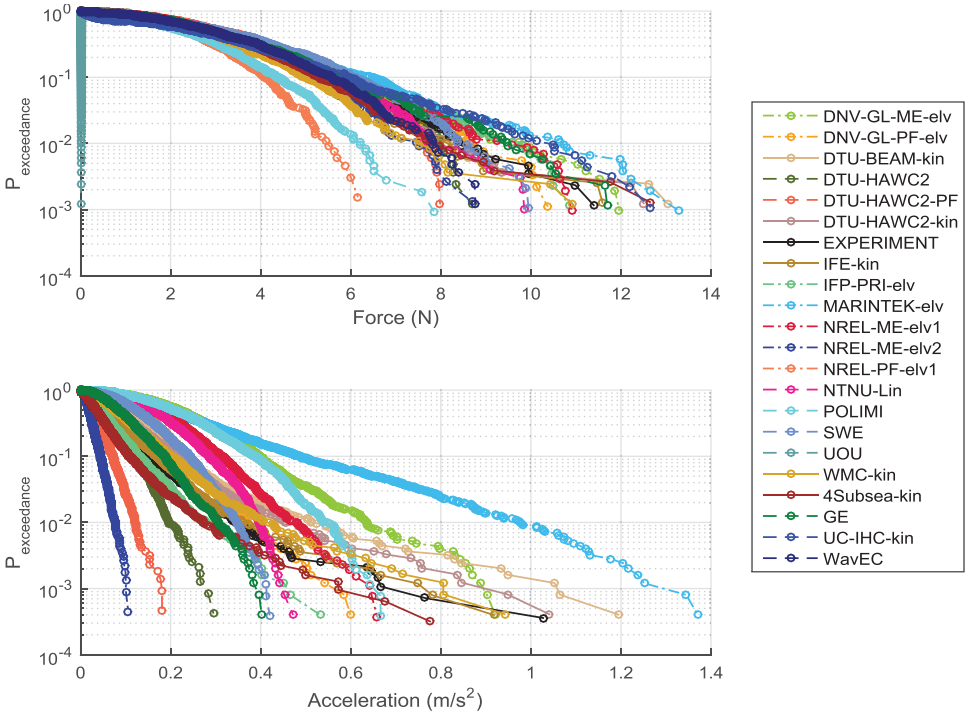

Figure 14. Validation of simulated exceedance probabilities for force and acceleration against test measurements(Test 4)

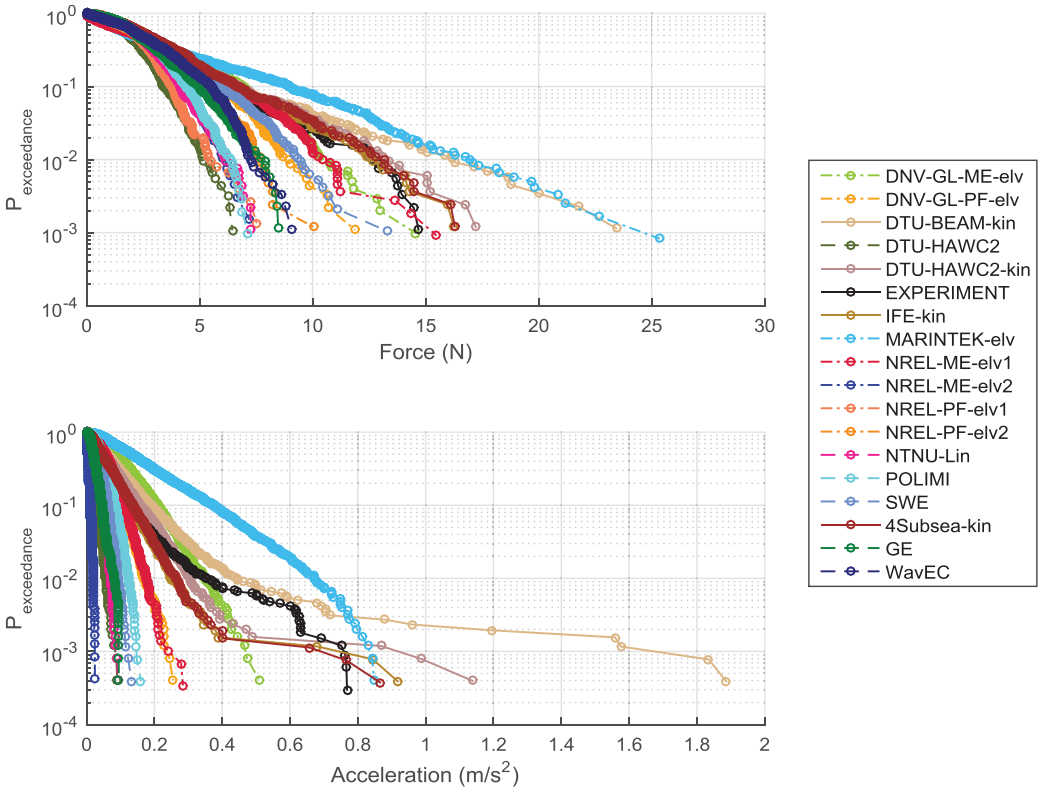

Figure 15. Validation of the simulated exceedance probabilities for the force and acceleration against the test measurements (Test 7)

6. Conclusions

Through this benchmark study, researchers made first steps in understanding the capabilities of available offshore wind modelling tools in accurately predicting the hydrodynamic loading and acceleration response of a flexible cylinder. The cylinder examined was created as a scaled version of the OC3 monopile, and is therefore representative of the types of structures that are used to support offshore wind turbines in shallow water. A sloped seabed was employed in the testing to help develop more nonlinear and breaking-type waves that are a concern in the design of these systems. The ability of these offshore wind modelling tools to accurately predict the hydrodynamic loads and acceleration response of a monopile-type structure was assessed through validation against a set of seven tank tests performed at DHI at two water depths, using both regular and irregular waves.

The first finding from this work is that higher-order wave theory is important in capturing the higher-order components of the hydrodynamic force, which could be important in predicting the extreme loads on the structure and potential excitation of structural frequencies. For the tests (1 and 2) that involved the cylinder excited by regular waves in deeper water, all codes calculated the overall magnitude of the force on the cylinder fairly consistently and well. The magnitude is dominated by the 1st-order component of the force because the waves are fairly linear, and all codes are good at capturing the 1st-order component. Codes using lower-order wave models cannot capture the higher-order components of the force, but this does not affect the overall force magnitude significantly in deep water. For the tests involving the cylinder in shallower water, the waves are less linear, and higher-order components of the waves and resulting force become much more important in accurately calculating the overall force on the structure. In addition, the harmonics of the force (if large enough) can potentially excite natural frequencies in the structure. Thus, it is important to capture these forces as they could lead to fatigue issues for the structure.

The second finding is that the complexity of nonlinear wave transformation over a sloped seabed (for this case) has shown a potential need for higher-fidelity approaches to accurately model the wave kinematics. A sloped seabed was used in this experiment to create strong wave nonlinearity by transformation to smaller depths. The sloped bed, however, also created wave kinematics (distributed wave velocities and accelerations) that cannot be approximated as well by standard wave theories that consider a flat bottom. Although this slope of 1:25 is much steeper than a realistic seabed, some level of slope or seabed nonuniformity will be present in real-world applications and wave transformation from deep water to the actual depth will inevitably be nonlinear. This study found that those able to model the sloped seabed and nonlinear wave transformation were able to more accurately represent the resulting distribution of forces and accelerations versus those using standard wave theories to derive the kinematics, including those using direct measurements of the wave elevation. It may be impractical computationally to derive wave kinematics from FNPF or CFD to perform a loads analysis of an offshore wind turbine, but these results can help show the level of influence the nonlinear wave transformation and seabed slope can have such that a more detailed analysis with FNPF or CFD might be warranted for certain conditions.

The third finding is that offshore wind modelling tools do not presently capture the total force applied to the structure during a breaking wave event. Through higher-order wave models and FNPF approaches, the highly nonlinear nature of the waves for shallow water conditions can be well approximated, but not the force that results when a wave breaks. A breaking wave will impart an impulsive load on the structure that will cause broad-band excitation of the structural frequencies. Participants are therefore moving towards including an impulsive force in their tools to approximate the loading of a breaking wave when breaking wave conditions are identified.

The group will now move on to examine more complex structures in the subsequent phases of the OC5 project. For Phase II, the group will validate the global dynamic response of a floating wind turbine supported by a semisubmersible tested at $1/50^{th}$ scale in a tank. The work performed for Phase I will be beneficial in understanding the differences in the forces and motion of this more complicated structure, which includes shadowing from multiple members and interaction from attached members of different sizes, as well as the complication of modelling a floating (moving) system. For Phase III, the group will validate the loads and response of a fixed-bottom, open-ocean offshore wind system.

Acknowledgements

We would like to acknowledge Ole Petersen at DHI and Henrik Bredmose and Michael Borg at DTU for graciously supplying the data, FNPF kinematics, and information needed for this first phase of the OC5 project. This work was supported by the U.S. Department of Energy under Contract No. DE-AC36-08GO28308 with the National Renewable Energy Laboratory. Funding for the work was provided by the DOE Office of Energy Efficiency and Renewable Energy, Wind and Water Power Technologies Office.

The U.S. Government retains and the publisher, by accepting the article for publication, acknowledges that the U.S. Government retains a nonexclusive, paid-up, irrevocable, worldwide license to publish or reproduce the published form of this work, or allow others to do so, for U.S. Government purposes.

References

[1] Robertson, A. et al. OC5 Project Phase I: Validation of Hydrodynamic Loading on a Fixed Cylinder. Presented at The International Society of Offshore and Polar Engineers Conference, June 2015; NREL Report No. CP-5000-63567.

[2] Bredmose, H. Mariegaard, J., Paulsen, B.T., Jensen, B., Schløer, S., Larsen, T.J., Kim, T. and Hansen, A.M. The Wave Loads project. Final report for the ForskEL 10495 Wave Loads project. DTU Wind Energy Report E-0045, December 2013.

[3] Bredmose, H., Slabiak, P., Sahlberg-Nielsen, L. & Schlütter, F. Dynamic excitation of monopiles by steep and breaking waves. Experimental and numerical study. Proc. of the ASME 32st 2013 Int. Conf. on Ocean, Offshore and Arctic Engineering, ASME.

[4] Nielsen, A., Schlütter, F., Sørensen, J. & Bredmose, H. Wave loads on a monopile in 3D waves. Proc. of the ASME 31st 2012 Int. Conf. on Ocean, Offshore and Arctic Engineering, ASME.

[5] Schlütter, F. Wave loads on offshore wind turbine foundations; Experiment description. Technical report, DHI, 2013.
[6] Jonkman, J. and Musial, M. Offshore Code Comparison Collaboration (OC3) for IEA Task 23 Offshore Wind Technology and Deployment. Technical Report NREL/TP-5000-48191, 2010.
[7] Morison, J. R.; O'Brien, M. P.; Johnson, J. W.; Schaaf, S. A. The force exerted by surface waves on piles. Petroleum Transactions (American Inst. of Mining Engineers) 1950; 189, 149–154.
[8] Gudmestad, Ove T.; Moe, Geir. Hydrodynamic coefficients for calculation of hydrodynamic loads on offshore truss structures. Marine Structures 1996; 9, 745–758.
[9] Sarpkaya, T.; Isaacson, M. Mechanics of wave forces on offshore structures. New York: Van Nostrand Reinhold, ISBN 0-442-25402-4, 1981.
[10] Engsig-Karup, A., Bingham, H.B., Lindberg, O. An efficient flexible-order model for 3D nonlinear water waves. J Comp Phys 2009; 228:2100–2118.
[11] Duncan P.E., Drake K.R. A note on simulation and analysis of irregular non-linear waves. App. Ocean Res. 1995;17:1-8.
[12] Bredmose, H. et. al. DeRisk - Accurate prediction of ULS wave loads; Outlook and first results. Energy Procedia XX (EERA DeepWind 2016).